COMPUTATIONAL STUDY OF NATURAL CONVECTION AND ENTROPY GENERATION IN 3-D CAVITY WITH ACTIVE LATERAL WALLS

by

Abdulwahab A. ALNAQI[a], Ahmed Kadhim HUSSEIN[b], Lioua KOLSI[c,d*], Abdullah A. A. A. AL-RASHED[a], Dong LI[e], and Hafiz Muhammad ALI[f]

[a] Department of Automotive and Marine Engineering Technology, College of Technological Studies, The Public Authority for Applied Education and Training, Adailiyah, Kuwait
[b] Mechanical Engineering Department, College of Engineering, University of Babylon, Babylon City, Hilla, Iraq
[c] College of Engineering, Mechanical Engineering Department, Hail University, Hail City, Saudi Arabia
[d] Unité de Métrologie et des Systèmes Énergétiques, École Nationale d'Ingénieurs 5000, Monastir, University of Monastir, Tunisia,
[e] School of Architecture and Civil Engineering, Northeast Petroleum University, Daqing, China
[f] Mechanical Engineering Department, King Fahd University of Petroleum and Minerals, Dhahean, Saudi Arabia

Original scientific paper
https://doi.org/10.2298/TSCI180810346A

Numerical simulation of the natural convection and entropy generation in an air-filled cubical cavity with active lateral walls is performed in this work. Both the lateral front and right sidewalls are maintained at an isothermal cold temperature. While an isothermal hot temperature is applied for both the lateral back and left sidewalls. The upper and lower walls are kept adiabatic. Entropy generation rates due to the fluid friction and the heat transfer are simulated by using the Second law of thermodynamics. Results are illustrated for Rayleigh numbers varied from ($10^3 \leq Ra \leq 10^6$). It was shown that the increase in the Rayleigh number leads to increase the average Nusselt number and to decrease the Bejan number. Also, it was found that both, S_{th}, and S_{tot}, increase slightly with the increase in Rayleigh number until they reach ($Ra = 10^5$) and then begin to jump after this value. After ($Ra = 10^5$), the increase in both, S_{tot}, and S_{fr}, is greater than S_{th}. Moreover, it was observed that iso-surfaces of S_{tot} are similar to S_{th} at ($10^3 \leq Ra \leq 10^5$), while they are similar to S_{fr} at high Rayleigh number.

Key words: *natural convection, 3-D flow, entropy generation, active lateral walls*

Introduction

Buoyancy driven flow or the natural convection phenomena in a cubical cavity has long been investigated because of its relevance to many practical industrial applications. These applications include solar collector receivers, aircraft cabin insulation, cooling of electronic equipment, nuclear reactor systems, atmospheric science applications, semi-conductor production, double pane windows, thermal storage systems and so on [1].

* Corresponding author, e-mail: lioua_enim@yahoo.fr

The natural convection was generated by density gradients, which are in most due to imposed external heat source [2]. In the available literature, various research works have been investigated both numerically and experimentally the natural convection in a 2-D cavities under different boundary conditions. Samples of these investigations include Aktas and Farouk [3], Hussain and Hussein [4], Corvaro *et al.* [5], Hussein *et al.* [6] and Maatki *et al.* [7].

From the another side, the number of papers related with the same problem but in a 3-D cavities were still much less than the corresponding works performed in a 2-D one. Fusegi *et al.* [8] investigated numerically the natural convection in a cubical cavity. The vertical side-walls of it were maintained at different temperatures. The other walls were kept insulated. It was found that the computed temperature and velocity profiles in the symmetry planes were greatly matched with the experimental investigations. Fusegi *et al.* [9] considered the same geometry and boundary conditions in Fusegi *et al.* [8] and they deduced that the Nusselt number for 3-D cavity was smaller than that for 2-D one at Ra < 10^5. Hiller *et al.* [10] performed a numerical and experimental study on the natural convection in a 3-D cavity with two isothermal walls maintained at a prescribed temperature. The experiments were performed at (Ra = $1.66 \cdot 10^5$ and Pr = 1109). Frederick [11] performed a numerical study about the natural convection in a cubical cavity with two active sectors on one vertical wall. His results indicated that Nusselt numbers became more than that computed for a side heated cavity at low values of Rayleigh number. Frederick and Berbakow [12] numerically studied the natural convection in a cubical enclosure with a hot source centered on a vertical wall and with an adjacent, fully cooled vertical wall. They concluded that the heat transfer had a weak dependent on the Rayleigh number. While it was greatly affected by the hot source mounted on the vertical wall. Oosthuizen *et al.* [13] studied numerically the natural convection in a 3-D rectangular enclosure. A hot rectangular element was inserted on the centre of one vertical walls of the enclosure, while the horizontal top surface of it was cooled to a uniform temperature. All another surfaces were insulated. The results showed that as Rayleigh number decreased, the relative change in the average Nusselt number with decreasing dimensionless width of the plate increased. Lo and Leu [14] investigated numerically by using a velocity-vorticity formulation the natural convection in an inclined cubic cavity for various values of Rayleigh number and inclination angles. Bocu and Altac [15] examined numerically the natural convection in 3-D rectangular enclosure, with pin arrays attached to its hot wall. The enclosure was heated from a lateral wall and cooled from the opposite one, while the other walls of it were adiabatic. The results explained that the Nusselt number ratio with respect to the enclosure without pins increased with pin length and its number. Onyango *et al.* [16] examined numerically by using a finite difference method, the natural convection in a 3-D square enclosure with a localized heating from below. The top and the two opposite vertical walls were maintained at a constant cold temperature. A heat source was fixed at the middle of the bottom wall. The other two vertical walls together with the non-heated part of the bottom wall were considered adiabatic. The results showed that the temperature was decreased as the fluid moved from the heat source towards the cold walls. Lee *et al.* [17] performed a numerical study of the natural convection in a differentially heated cubical enclosure filled with air. The right vertical sidewall was maintained at a hot temperature, while all another walls were kept cold. The flow and thermal characteristics of the natural convection were presented and discussed. Ahmadi [18] performed a numerical study about the laminar natural convection in a 3-D rectangular enclosure. The left and right vertical sidewalls were maintained at hot and cold temperatures respectively. The other walls were kept adiabatic. They investigated the effects of Rayleigh number, size and position of hot and cold sources on the flow and thermal characteristics inside the enclosure. It was found that the average Nusselt number together with the heat transfer rate from hot and cold sources were increased with increasing Rayleigh number. Additional useful researches related with the subject can be found in [19-33].

From the literature survey, it can be seen that no research available up to date studies the natural convection phenomena and the entropy generation in an air-filled cubical cavity with active lateral walls. In summary, this is the first original work which studied this problem in more details.

Geometry description

The 3-D natural convection problem inside an air filled (Pr = 0.71) cubical cavity is investigated numerically in the present paper. Both the lateral front and right sidewalls are maintained at cold temperature, T_c. An isothermal hot temperature, T_h, is applied for both the lateral back and left sidewalls. The upper and lower walls are kept adiabatic as shown in fig. 1. The flow inside the considered cavity is assumed unsteady, incompressible, laminar, 3-D and Newtonian. The thermo-physical properties of the fluid (except the density) are considered constant. The thermal and the flow fields are computed for ($10^3 \le \text{Ra} \le 10^6$) and the irreversibility coefficient is considered constant as ($\varphi = 10^{-4}$). The latter represents the relative importance of the fluid friction and heat transfer on the entropy generation rate.

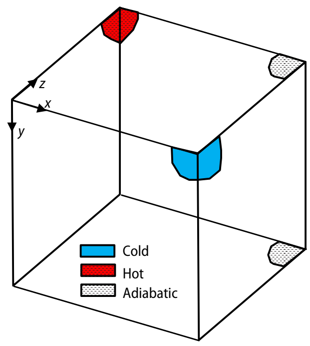

Figure 1. Schematic diagram of the present problem

Mathematical model, initial and boundary conditions and the numerical solution

In order to begin the mathematical modeling of the present problem and to cancel the pressure term in a 3-D cavity, the vector potential-vorticity formula ($\vec{\psi} - \vec{\omega}$) is adopted and is written:

$$\vec{\omega}' = \vec{\nabla} \times \vec{V}' \quad \text{and} \quad \vec{V}' = \vec{\nabla} \times \vec{\psi}' \tag{1}$$

The dimensionless governing equations can be constructed [23]:

$$-\vec{\omega} = \nabla^2 \vec{\psi} \tag{2}$$

$$\frac{\partial \vec{\omega}}{\partial t} + (\vec{V}\nabla)\vec{\omega} - (\vec{\omega}\nabla)\vec{V} = \Delta\vec{\omega} + \text{Ra}\,\text{Pr}\left[\frac{\partial T}{\partial z}; 0; -\frac{\partial T}{\partial x}\right] \tag{3}$$

$$\frac{\partial T}{\partial t} + \vec{V}\nabla T = \Delta T \tag{4}$$

where $\text{Pr} = \nu/\alpha$ and $\text{Ra} = g\beta\Delta T l^3/\nu\alpha$

The velocity, $\vec{V}'$, time, t', vector potential, $\vec{\psi}'$, and vorticity, $\vec{\omega}'$ are written in the dimensionless forms by α_f/l, α, and l^2/α_f.

The dimensionless temperature is written:

$$T = \frac{T' - T'_c}{T'_h - T'_c} \tag{5}$$

The initial conditions for the present geometry are:

$$T=0,\quad V_x=V_y=V_z=0 \quad \text{and} \quad \omega_x=\omega_y=\omega_z=0 \quad \text{at} \quad t=0$$

The boundary conditions are defined:
– Temperature:

$$T=1 \quad \text{at} \quad x=0 \quad \text{and} \quad z=1,\quad T=0 \quad \text{at} \quad x=1 \quad \text{and} \quad z=0,\quad \frac{\partial T}{\partial n}=0 \quad \text{at} \quad y=0 \quad \text{and} \quad y=1$$

– Vector potential:

$$\frac{\partial \psi_x}{\partial x}=\psi_y=\psi_z=0 \quad \text{at} \quad x=0 \quad \text{and} \quad 1,\quad \psi_x=\frac{\partial \psi_y}{\partial y}=\psi_z=0 \quad \text{at} \quad y=0 \quad \text{and} \quad 1$$

$$\psi_x=\psi_y=\frac{\partial \psi_z}{\partial z}=0 \quad \text{at} \quad z=0 \quad \text{and} \quad 1$$

– Velocity:

$$V_x=V_y=V_z=0 \quad \text{on all cavity walls.}$$

– Vorticity:

$$\omega_x=0,\quad \omega_y=-\frac{\partial V_z}{\partial x},\quad \omega_z=\frac{\partial V_y}{\partial x} \quad \text{at} \quad x=0 \quad \text{and} \quad 1,$$
$$\omega_x=\frac{\partial V_z}{\partial y},\quad \omega_y=0,\quad \omega_z=-\frac{\partial V_x}{\partial y} \quad \text{at} \quad y=0 \quad \text{and} \quad 1,$$
$$\omega_x=-\frac{\partial V_y}{\partial z},\quad \omega_y=\frac{\partial V_x}{\partial z},\quad \omega_z=0 \quad \text{at} \quad z=0 \quad \text{and} \quad 1$$

The dimensionless local generated entropy, N_s, is expressed as [23]:

$$N_s=\left[\left(\frac{\partial T}{\partial x}\right)^2+\left(\frac{\partial T}{\partial y}\right)^2+\left(\frac{\partial T}{\partial z}\right)^2\right]+\varphi\left\{2\left[\left(\frac{\partial V_x}{\partial x}\right)^2+\left(\frac{\partial V_y}{\partial y}\right)^2+\left(\frac{\partial V_z}{\partial z}\right)^2\right]+\right.$$
$$\left.+\left[\left(\frac{\partial V_y}{\partial x}+\frac{\partial V_x}{\partial y}\right)^2+\left(\frac{\partial V_z}{\partial y}+\frac{\partial V_y}{\partial z}\right)^2+\left(\frac{\partial V_x}{\partial z}+\frac{\partial V_z}{\partial x}\right)^2\right]\right\} \tag{5}$$

with φ is the irreversibility coefficient defined by $\varphi=\mu\alpha^2T_0/l^2k\Delta T^2$.

The first part in eq. (5) refers to the local generated entropy due to the temperature gradients and noted as, $N_{\text{s-th}}$. The second part of it refers to the local generated entropy due to the fluid friction and noted as, $N_{\text{s-fric}}$. Furthermore, the total dimensionless generated entropy, S_{tot}, is written:

$$S_{\text{tot}}=\int_v N_s \text{d}v=\int_v (N_{s\text{-th}}+N_{s\text{-fr}})\text{d}v=S_{\text{th}}+S_{\text{fr}} \tag{6}$$

The ratio of the thermal entropy to the total entropy is defined by the Bejan number:

$$\text{Be}=\frac{S_{\text{th}}}{S_{\text{th}}+S_{\text{fr}}} \tag{7}$$

The local and average Nusselt numbers are given:

$$\mathrm{Nu} = \left.\frac{\partial T}{\partial x}\right|_{\mathrm{hot}\_S} \quad \text{and} \quad \mathrm{Nu}_{\mathrm{av}} = \int_S \mathrm{Nu}\,\mathrm{d}s \tag{8}$$

Numerical approach and code verification

The solution of the governing eqs. (2)-(5) is performed numerically using the control volume technique. The alternating direction implicit scheme is used to discretize the temporal derivatives, while the central-difference approach is used to deal with the convection parts in the governing equations. The solution is considered fair when the following convergence criterion is satisfied for each step of time:

$$\sum_{i}^{1,2,3} \frac{\max\left|\psi_i^n - \psi_i^{n-1}\right|}{\max\left|\psi_i^n\right|} + \max\left|T_i^n - T_i^{n-1}\right| \le 10^{-5} \tag{9}$$

In order to verify the accuracy of our computer program, the natural convection problems in a differentially heated cubical cavity which are studied previously by Wakashima and Saitoh [34] and Fusegi *et al.* [35] are re-solved again by our computer program. Table 1 shows a comparison between these results for various values of Rayleigh number. The results of the comparison indicate a very good matching between the results computed by our computer program with their corresponding results given by Wakashima and Saitoh [34] and Fusegi *et al.* [35], respectively. This verification gives a good confidence in the present computer program to investigate with the current problem.

Table 1. Comparison of present results with the 3-D results of [34] and [35] for differentially heated cubic closed space and Pr = 0.71

Ra	Authors	$V_{x\max}(y)$	$V_{y\max}(x)$	$\mathrm{Nu}_{\mathrm{av}}$
10^4	Present work	0.199(0.826)	0.221 (0.112)	2.062
	[34]	0.198 (0.825)	0.222 (0.117)	2.062
	[35]	0.201 (0.817)	0.225 (0.117)	2.1
10^5	Present work	0.143 (0.847)	0.245 (0.064)	4.378
	[34]	0.147 (0.85)	0.246 (0.068)	4.366
	[35]	0.147 (0.855)	0.247 (0.065)	4.361
10^6	Present work	0.0832(0.847)	0.254 (0.032)	8.618
	[34]	0.0811 (0.86)	0.2583(0.032)	8.6097
	[35]	0.0841(0.856)	0.259(0.033)	8.77

The average Nusselt number on the hot walls was selected as a sensitive parameter. Results of the grid sensitivity analysis are shown in tab. 2. The incremental increase in the percentage of $\mathrm{Nu}_{\mathrm{av}}$ for grids of 81^3 to 91^3 is only 0.143%. Hence, considering the computational economy and accuracy, a spatial mesh size of 81^3 and a time-step of 10^{-3} were opted for the present study. For all executions the solution is stored at $t = 2$.

Results and discussion

The laminar 3-D natural convection and entropy generation in an air-filled cubical cavity with active lateral walls is simulated numerically in the present research. The effect of

Table 2. Grid sensitivity analysis for Pr = 0.7 and Ra = 10^5

Grid size	Nu_{avg}	Percentage increase	Incremental increase
61^3	4.8401	–	–
71^3	4.9205	1.6611	–
81^3	4.9639	2.5431	0.8820
91^3	4.971	2.6861	0.1430

Rayleigh number on the flow and thermal fields, heat transfer and entropy generation has been investigated. The results were illustrated by trajectory of particles, iso-surfaces of temperature, average Nusselt number, iso-surfaces of the entropy generations and the Bejan number. Figure 2 shows the 3-D trajectory of particles for different values of Rayleigh number. According to the buoyancy force effect, the convection currents begin from the hot lateral back and left sidewalls until they reach to the adiabatic upper wall. After that, they reverse their direction and move towards the cold lateral front and right sidewalls. Then, they reach again to the hot walls after passing the adiabatic lower wall.

This repeated rotation of the convection currents lead to produce the convection vortices which occupy the entire cavity as seen in fig. 2. For low Rayleigh number (Ra = 10^3) or when the effect of the buoyancy force which is due to the temperature difference inside the cavity is weak. The shapes of convection vortices are symmetrical and extend laterally between the hot and cold lateral walls. In this case, the natural convection role in the heat transfer pro-

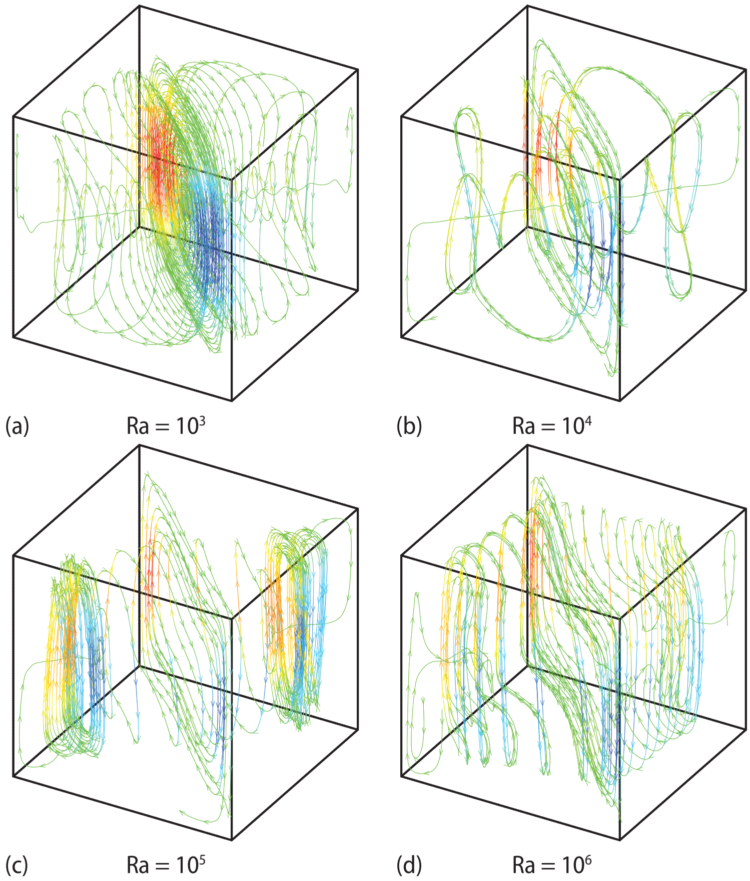

Figure 2. Particle trajectories for various Rayleigh number

cess is slight, while the conduction is predominant. Now, as the Rayleigh number increases gradually, the intensity of the flow circulation begins to increase. In this case, the viscous forces become smaller than the buoyancy one. Therefore, a clear dissipation in the convection vortices towards all the cavity walls can be observed. For this reason, their shapes are greatly deformed as the Rayleigh number increases. When the natural convection becomes predominant or when (Ra = 10^6), the shape of vortices was highly deformed in comparison with their corresponding vortices which are seen at (Ra = 10^3). Moreover, it can be noticed from the results of fig. 2 that the flow circulation is stronger near the center of the cavity and slight at the lateral cold and hot walls due to non- slip boundary conditions.

From the other side, the effect of the Rayleigh number on the temperature field is apparent from the iso-surfaces of temperature as illustrated in fig. 3. When the effect of the natural convection is weak or when the Rayleigh number is low (Ra = 10^3), the iso-surfaces of temperature are uniform, symmetrical, smooth and parallel to the cavity sidewalls. It can be observed from fig. 3, that iso-surfaces of temperature emanate from the lateral back and left sidewalls (*i. e.*, hot walls) until they arrive to the cold lateral front and right sidewalls, indicating the path of the thermal field. Heat conduction is the dominant mode of the heat transfer inside the cubical cavity. Now, when the natural convection effect becomes dominant or when the Rayleigh number increases gradually from Ra = 10^4 to Ra = 10^6, the iso-surfaces of temperature become wavy , curved and clustered to the lateral hot back and left sidewalls as illustrated from fig. 3. Moreover, it can be noticed a stagnant region from iso-surfaces of temperature at the upper part of the cubical lateral cavity and this region begins to decrease as the Rayleigh number increases.

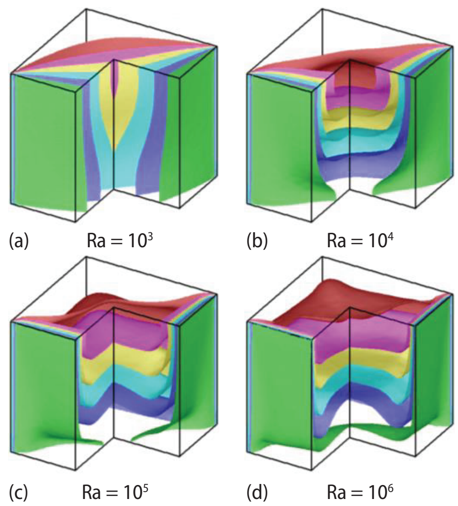

Figure 3. Temperature contours for various values of Rayleigh number

Figure 4 illustrates the behavior of the average Nusselt number, Nu_{av}, in the cubical lateral cavity for different values of the Rayleigh number. It can be seen that, when the Rayleigh number is low (Ra = 10^3), the values of Nu_{av} is low also. This refers that the heat is transferred inside the lateral cavity by the conduction. After that, a clear increasing in the values of the, Nu_{av}, can be observed as the Rayleigh number increases. This increasing can be returned to the high effect of the natural convection. At (Ra = 10^6), the values of Nu_{av} reach their maximum range which reflect the strong effect of the natural convection inside the cavity.

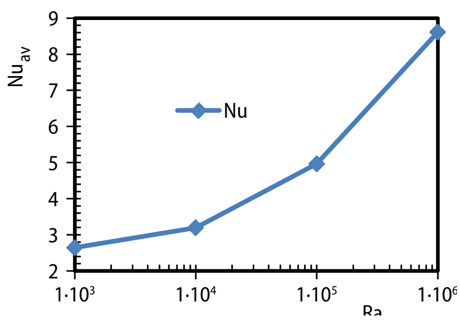

Figure 4. Variation on Nu_{av} *vs.* Ra

Figure 5 displays iso-surfaces of the entropy generations and the Bejan number in the cubical lateral cavity for different values of the Rayleigh number. For ($10^3 \leq$ Ra $\leq 10^5$), the S_{th} iso-surfaces are symmetrical and distributed vertically near the lateral cavity walls. But, for

(Ra = 10^6), it can be seen that S_{th} iso-surfaces extend also in the (x-z) plane due to the increase in the heat transfer losses with increasing of Rayleigh number.

This leads to increase the S_{th}. Furthermore, it can be observed that S_{th} iso-surfaces increase adjacent the lateral cavity walls due to the temperature difference. While, they absent at the adiabatic upper and lower walls. Moreover, it can be observed from fig. 5, that there is a space region in the center of the cavity. This is because of the stagnant or low velocity of the fluid. With respect to the iso-surfaces of S_{fr}, it can be seen that they are concentrated intensely adjacent the cavity walls. This is due to the high effect of the friction between the fluid inside the cavity and its walls. For iso-surfaces of S_{tot}, it is interesting to see that their behavior is similar to that seen for S_{th} at ($10^3 \le \text{Ra} \le 10^5$). This refers to the dominance of S_{th} or in another words the domination of the irreversibility due to the heat transfer at this range of Rayleigh number. But, at (Ra = 10^6), the iso-surfaces of S_{tot} try to be similar to S_{fr}. This behavior can be returned to the dominance of the irreversibility due to the fluid friction at high Rayleigh number.

Figure 5 illustrates iso-surfaces of the Bejan number for various values of the Rayleigh number. The Bejan number is a dimensionless number which is used to measure the relative magnitude of the heat transfer and fluid friction irreversibilities. High values of Bejan number indicate the dominance of thermal generated entropy and low values indicate the frictional one. When the Rayleigh number is low (Ra = 10^3), the iso-surfaces of the Bejan number have a high intense and distribute uniformly on the lateral walls of the cavity.

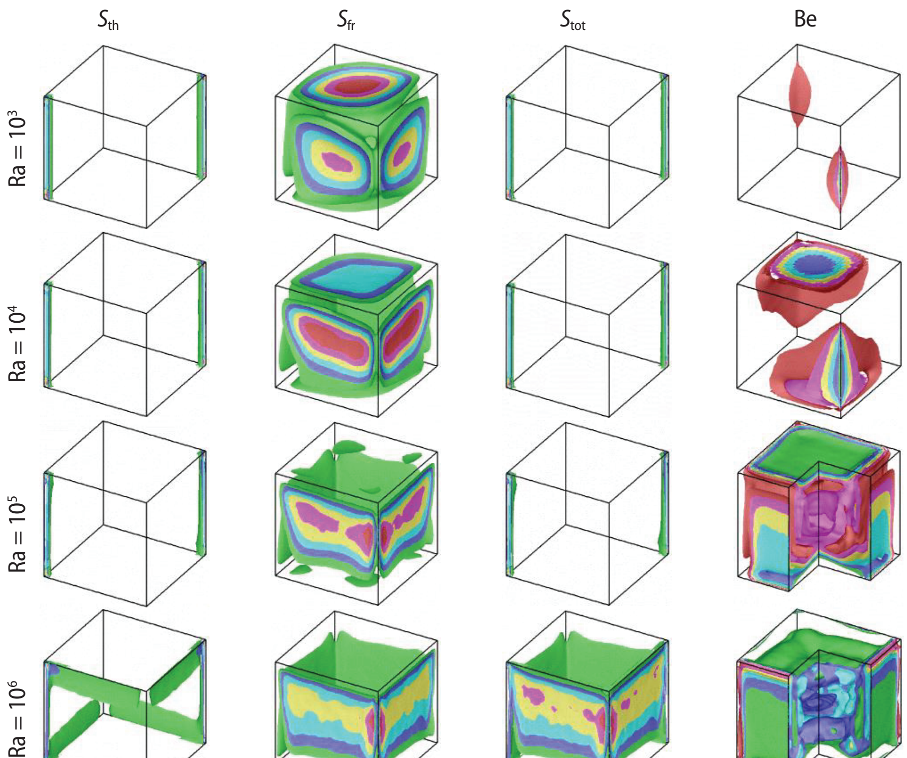

Figure 5. Iso-surfaces of the entropy generations and Bejan number in the cubical lateral cavity for different values of Rayleigh number

As Rayleigh number increases, they begin to move towards the center of the cavity. At (Ra = 10^6), the intensity of the Bejan number iso-surfaces around the lateral walls of the cavity begin to decrease in comparison with their corresponding iso-surfaces which are observed when the Rayleigh number is low.

Figure 6 demonstrates the variation of various entropies generation, S_{th}, S_{fr}, and, S_{tot}, in the cubical lateral cavity for different values of the Rayleigh number. It can be observed that the entropy generation rate due to the fluid friction, S_{fr}, remains approximately constant as the Rayleigh number increases up to (Ra = 10^5). After that, it increases strongly with the increase in the Rayleigh number. From the opposite side, both the entropy generation due to the heat transfer, S_{th}, and the total entropy generation, S_{tot}, increase slightly with the increase in the Rayleigh number until they reach (Ra = 10^5) and then begin to jump after this value. This jumping is strong for, S_{tot}, and slight for S_{th}. The behavior noticed at ($10^3 \leq \text{Ra} \leq 10^5$) can be returned to the high increase in the heat transfer losses and weak increase in the friction between the fluid inside the cavity and its different walls. After (Ra = 10^5), the increase in both, S_{tot} and S_{fr}, is greater than S_{th} which indicates a reduction in the heat transfer losses. For this reason, the peak value of the total entropy generation, S_{tot}, and entropy generation due to friction, S_{fr}, occurs at the maximum value of Rayleigh number (*i. e.*, Ra = 10^6).

Finally, fig. 7 illustrates the behavior of the Bejan number for different values of the Rayleigh number. The results display that as the Rayleigh number increases, the values of the Bejan number begin to decrease. Since, for high values of Rayleigh number the increase in, S_{tot}, is much higher than the increase in, S_{th}, as explained previously in fig. 6. This leads of course to decrease the values of the Bejan number. Furthermore, an interesting behavior can be observed in fig. 7, where there is a linear variation between the Bejan and Rayleigh numbers for low range of Rayleigh number. Therefore, it can be concluded that for low values of Rayleigh number most of the total entropy generation S_{tot} is due to the heat transfer losses or S_{th} or in another words, the friction losses or S_{fr} are very weak. This leads to make the values of the Bejan number approximately unity for low range of Rayleigh number as displayed in fig. 7.

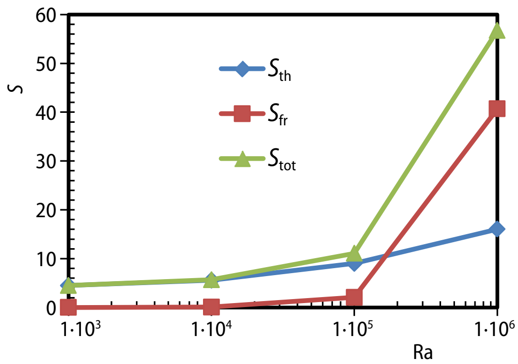

Figure 6. Variations of various entropies generation in the cubical lateral cavity for different values of Rayleigh number

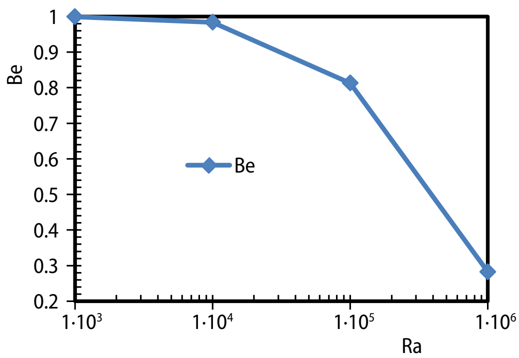

Figure 7. Variation of Bejan number in the cubical lateral cavity for different values of Rayleigh number

Conclusion

In this paper, natural convection and entropy generation in 3-D cavity having active lateral wall is investigated numerically using the finite volume method. The following conclusions can be highlighted from the results of the present work.

- The shape of the flow vortices greatly affected by the variation of Rayleigh number.
- Iso-surfaces of temperature are uniform, smooth and parallel to the cavity sidewalls when Rayleigh number is low. As Rayleigh number increases, they become wavy, curved and clustered to the lateral back and left sidewalls.
- The values of the average Nusselt number increase as the Rayleigh number increases.
- Entropy generation due to fluid friction, S_{fr}, remains approximately constant as Rayleigh number increases up to Ra = 10^5. After that, it increases strongly with the increase in Rayleigh number.
- Both the entropy generation due to heat transfer, S_{th}, and total entropy generation, S_{tot}, increase slightly with the increase in Rayleigh number until they reach Ra = 10^5 and then begin to jump after this value. After Ra = 10^5, the increase in both, S_{tot} and S_{fr}, is greater than S_{th}.
- Bejan number increases as the Rayleigh number decreases.
- Iso-surfaces of S_{th} are symmetrical and distributed vertically near the lateral cavity walls for ($10^3 \leq$ Ra $\leq 10^5$). But, for (Ra = 10^6), they try to extend also in the (x-z) plane.
- Iso-surfaces of S_{fr} are high adjacent the cavity walls.
- Iso-surfaces of S_{tot} are similar to S_{th} at ($10^3 \leq$ Ra $\leq 10^5$), while they are similar to S_{fr} at high Rayleigh number.

Acknowledgment

The authors would like to acknowledge the research deanship of University of Ha'il, KSA for funding the project "RG-191225".

Nomenclature

Be – Bejan number, [–]
g – acceleration due to gravity, [ms^{-2}]
k – thermal conductivity, [Wm^{-1}K^{-1}]
l – cavity width and height, [m]
N_s – dimensionless local generated entropy
Nu – Nusselt number, [–]
Pr – Prandtl number, [–]
$\vec{q}$ – heat flux vector, [Wm^{-2}]
Ra – Rayleigh number, [–]
S'_{gen} – generated entropy per unit volume, [Wm^{-3}K^{-1}]
S_{th} – thermal entropy, [Wm^{-3}K^{-1}]
S_{tot} – total entropy, [Wm^{-3}K^{-1}]
t – dimensionless time, ($= t'\alpha/l^2$), [–]
T – dimensionless temperature, [$= (T' - T'_c)/(T'_h - T'_c)$], [–]
ΔT – dimensionless temperature difference, [–]
T'_c – cold temperature, [K]
T'_h – hot temperature, [K]
T_o – average temperature, [$= (T'_c + T'_h)/2$], [K]
$\vec{V}$ – dimensionless velocity vector, ($= \vec{V}'l/\alpha$), [–]
x, y, z – dimensionless Cartesian co-ordinates, ($= x'/l, y'/l, z'/l$), [–]

Greek symbols

α – thermal diffusivity, [m^{2}s^{-1}]
β – thermal expansion coefficient, [K^{-1}]
μ – dynamic viscosity, [kgm^{-1}s^{-1}]
ν – kinematic viscosity, [m^{2}s^{-1}]
φ – irreversibility coefficient
$\vec{\psi}$ – dimensionless vector potential, ($= \vec{\psi}'/\alpha$), [–]
$\vec{\omega}$ – dimensionless vorticity, ($= \vec{\omega}'\alpha/l^2$), [–]
ϕ' – dissipation function

Subscripts

av – average
c – cold
h – hot
x, y, z – Cartesian co-ordinates
fr – friction
th – thermal
tot – total

Superscript

$'$ – dimensional variable

References

[1] Ghachem, K., *et al.*, Numerical Simulation of Three-Dimensional Double Diffusive Free Convection Flow and Irreversibility Studies in a Solar Distiller, *International Communications in Heat and Mass Transfer, 39* (2012), 6, pp. 869-876

[2] Ahmed, S., *et al.*, Viscous Dissipation and Radiation Effects on MHD Natural Convection in a Square Enclosure Filled with a Porous Medium, *Nuclear Engineering and Design, 266* (2014), Jan., pp. 34-42

[3] Aktas, M., Farouk, B., Numerical Simulation of Developing Natural Convection in an Enclosure Due to Rapid Heating, *International Journal of Heat and Mass Transfer, 46* (2003), 12, pp. 2253-2261

[4] Hussain, S., Hussein, A. K., Numerical Investigation of Natural Convection Phenomena in a Uniformly Heated Circular Cylinder Immersed in Square Enclosure Filled with Air at Different Vertical Locations, *International Communications in Heat and Mass Transfer, 37* (2010), 8, pp. 1115-1126

[5] Corvaro, F., *et al.*, Experimental PIV and Interferometric Analysis of Natural Convection in a Square Enclosure with Partially Active Hot and Cold Walls, *International Journal of Thermal Sciences, 50* (2011), 9, pp. 1629-1638

[6] Hussein, A. K., *et al.*, Modeling of MHD Natural Convection in a Square Enclosure Having an Adiabatic Square Shaped Body Using Lattice Boltzmann Method, *Alexandria Engineering Journal, 55* (2016), 1, pp. 203-214

[7] Maatki, C., *et al.*, Inclination Effects of Magnetic Field Direction in 3D Double-Diffusive Natural Convection, *Applied Mathematics and Computation, 273* (2016), Jan., pp. 178-189

[8] Fusegi, T., *et al.*, A Numerical Study of 3D Natural Convection in a Cube: Effects of the Horizontal Thermal Boundary Conditions, *Fluid Dynamics Research, 8* (1991), 5-6, pp. 221-230

[9] Fusegi, T., *et al.*, A Numerical Study of Three-Dimensional Natural Convection in a Differentially Heated Cubical Enclosure, *International Journal of Heat and Mass Transfer, 34* (1991), 6, pp. 1543-1557

[10] Hiller, W., *et al.*, Onset of Natural Convection in a Cube, *International Journal of Heat and Mass Transfer, 36* (1993), 13, pp. 3251-3263

[11] Frederick, R., Natural Convection Heat Transfer in a Cubical Enclosure with Two Active Sectors on One Vertical Wall, *International Communications in Heat and Mass Transfer, 24* (1997), 4, pp. 507-520

[12] Frederick, R., Berbakow, O., Natural Convection in Cubical Enclosures with Thermal Sources on Adjacent Vertical Walls, *Numerical Heat Transfer, Part A, 41* (2002), 3, pp. 331-340

[13] Oosthuizen, P., *et al.*, Three-Dimensional Natural Convective Flow in a Rectangular Enclosure with a Rectangular Heated Section on One Vertical Wall and a Cooled Horizontal Upper Wall, *Proceedings*, 5th European Thermal-Sciences Conference, Eindhoven, Netherlands, 2008, pp. 1-8

[14] Lo, D., Leu, S., DQ Analysis of 3D Natural Convection in an Inclined Cavity Using an Velocity-Vorticity Formulation, *Proceedings of World Academy of Science, Engineering and Technology, 36* (2008), pp. 370-375

[15] Bocu, Z., Altac, Z., Laminar Natural Convection Heat Transfer and Air Flow in Three-Dimensional Rectangular Enclosures with Pin Arrays Attached to Hot Wall, *Applied Thermal Engineering, 31* (2011), 16, pp. 3189-3195

[16] Onyango, O., *et al.*, Enhancement of Natural Convection Heat Transfer in a Square Enclosure with Localized Heating from Below, *International Journal of Science and Research, 2* (2013), 10, pp. 82-87

[17] Lee, H., *et al.*, A Numerical Study of Three-Dimensional Natural Convection in a Differentially Heated Cubical Enclosure, *Proceedings,* International Conference on Mechanics, Fluids, Heat, Elasticity and Electromagnetic Fields, Venice, Italy, 2013, pp. 111-115

[18] Ahmadi, M., Fluid Flow and Heat Transfer Characteristics of Natural Convection in Square 3-D Enclosure Due to Discrete Sources, *World Applied Sciences Journal, 29* (2014), 10, pp. 1291-1300

[19] Kolsi, L., *et al.*, Computational Analysis of Three-Dimensional Unsteady Natural Convection and Entropy Generation in a Cubical Enclosure Filled with Water-Al_2O_3 Nanofluid, *Arabian Journal for Science and Engineering, 39* (2014), 11, pp. 7483-7493

[20] Hussein, A. K., *et al.*, Three-Dimensional Unsteady Natural Convection and Entropy Generation in an Inclined Cubical Trapezoidal Cavity with an Isothermal Bottom Wall, *Alexandria Engineering Journal, 55* (2016), 2, pp. 741-755

[21] Al-Rashed, A., *et al.*, Numerical Study of Three-Dimensional Natural Convection and Entropy Generation in a Cubical Cavity with Partially Active Vertical Walls, *Case Studies in Thermal Engineering, 10* (2017), Sept., pp. 100-110

[22] Al-Rashed, A., *et al.*, Mixed Convection and Entropy Generation in a Nanofluid Filled Cubical Open Cavity with a Central Isothermal Block, *International Journal of Mechanical Sciences, 135* (2018), Jan., pp. 362-375

[23] Kolsi, L., *et al.*, Second Law Analysis in a Three-Dimensional Lid-Driven Cavity, *International Communications in Heat and Mass Transfer, 38* (2011), 10, pp. 1376-1383

[24] Oztop, H. F., Al-Salem, K., A Review on Entropy Generation in Natural and Mixed Convection Heat Transfer for Energy Systems, *Renewable and Sustainable Energy Reviews, 16* (2012), 1, pp. 911-920

[25] Mahian, O., *et al.*, Entropy Generation between Two Vertical Cylinders in the Presence of MHD Flow Subjected to Constant Wall Temperature, *International Communications in Heat and Mass Transfer, 44* (2013), May, pp. 87-92
[26] Sheremet, M. A., *et al.*, Analysis of Entropy Generation in Natural Convection of Nanofluid Inside a Square Cavity Having Hot Solid Block: Tiwari and Das' Model, *Entropy, 18* (2015), 1, 9
[27] Selimefendigil, F., Oztop, H. F., MHD Mixed Convection and Entropy Generation of Power Law Fluids in a Cavity with a Partial Heater under the Effect of a Rotating Cylinder, *International Journal of Heat and Mass Transfer, 98* (2016), July, pp. 40-51
[28] Mahian, O., *et al.*, Recent Advances in Modeling and Simulation of Nanofluid Flows-Part I: Fundamental and Theory, *Phys. Rep., 790* (2019), Feb., pp. 1-48
[29] Mahian, O., *et al.*, Recent Advances in Modeling and Simulation of Nanofluid Flows-Part I: Fundamental and Theory, *Phys. Rep., 791* (2019), Feb., 1-59
[30] Kolsi, L., *et al.*, The Effect of an External Magnetic Field on the Entropy Generation in Three-Dimensional Natural Convection, *Thermal Science, 14* (2010), 2, pp. 341-352
[31] Rahimi, A., *et al.*, Experimental and Numerical Study on Heat Transfer Performance of Three-Dimensional Natural Convection in an Enclosure Filled with DWCNTs-Water Nanofluid, *Powder Technology, 322* (2017), Dec., pp. 340-352
[32] Kasaeipoor, A., *et al.*, Free Convection Heat Transfer and Entropy Generation Analysis of MWCNT-MgO (15%-85%)/Water Nanofluid Using Lattice Boltzmann Method in Cavity with Refrigerant Solid Body – Experimental Thermo-Physical Properties, *Powder Technology, 322* (2017), Dec., pp. 9-23
[33] Abidi, A., *et al.*, Effect of Radiative Heat Transfer on Three-Dimensional Double Diffusive Natural Convection, *Numerical Heat Transfer, Part A: Applications, 60* (2011), 9, pp. 785-809
[34] Wakashima, S., Saitoh, T., Benchmark Solutions for Natural Convection in a Cubic Cavity Using the High-Order Time-Space Method, *International Journal of Heat and Mass Transfer, 47* (2004), 4, pp. 853-864
[35] Fusegi, T., *et al.*, Numerical Study of 3D Natural Convection in a Cube: Effects of the Horizontal Thermal Boundary Conditions, *Fluid Dynamics Research, 8* (1991), 5-6, pp. 221-230

Paper submitted: August 10, 2018
Paper revised: November 25, 2018
Paper accepted: November 28, 2018